ESTIMATION OF DAILY GLOBAL SOLAR IRRADIANCE FROM HIMAWARI-8 PRODUCTS OVER CHINA

Yanli Zhang[1,*], Linhong Chen[2, 1], Jingfeng Liu[1]
[1] College of Geography and Environment Science, Northwest Normal University, Lanzhou 730070, China
[2] Yunfu Urban and Rural Planning Research Center, Yunfu 527300, China

Commission III, WG III/10

KEY WORDS: Himawari-8, Global solar irradiance, Gaussian fitting, Geostationary satellite, Polar-orbiting satellite, Python.

ABSTRACT:

Daily global surface solar irradiance (SSI) is of great importance parameter in the surface energy balance, climate modelling, and solar energy utilization. However, it is still challenging to extend the estimated instantaneous solar radiation to the daily global SSI from either geostationary satellites or polar-orbiting satellites. In this study, a method for estimating the daily global SSI is proposed based on the Himawari-8 hourly SSI products using pixel-by-pixel Gaussian fitting to simulate the diurnal SSI variation. Compared with ground-based observations, the daily global SSI estimated by Gaussian fitting have higher accuracy under various weather conditions than by the simple accumulation or quadratic polynomials, and the coefficient of determination (R2) between the estimated and observed values exceeds 0.86. The verification results also show different estimation accuracies under different weather conditions. The root-mean-square errors (RMSEs) under clear-sky and all-sky conditions are 2.36 MJ/m2 and 3.06 MJ/m2, respectively. In addition, experimental results show that the daily global SSI in China has high spatial heterogeneity. For higher-elevation areas with low cloud cover, such as the Qinghai-Tibet Plateau, Inner Mongolia, and Northwest China, the daily global SSI is higher than other areas. In contrast, the values of daily global SSI is relatively low in the eastern regions of Southwest and Northeast China.

1. INTRODUCTION

Daily global surface solar irradiance (SSI) is an essential parameter affecting surface-atmosphere interactions, hydrological modelling, and snow/glacial melting simulation models (Yang and Koike, 2005; Journée et al., 2010; Huang et al., 2019; Hou et al., 2019). SSI means shortwave solar radiation received by a given surface, which can be obtained through empirical or physical models based on meteorological observations. However, the SSI spatial distribution has been shown to be inadequate for many applications due to the limited number of ground stations. Nowadays, both polar-orbiting satellites and geostationary satellites can obtain surface and atmospheric information and thus can provide solar irradiance products with various temporal and spatial resolutions (Zhang et al., 2020). However, it is still challenging to obtain daily global SSI with a high spatiotemporal resolution.

Polar-orbiting satellites such as MODIS can retrieve SSI with higher spatial resolution, however, these radiation products have a limited temporal resolution. Numerous studies have made great efforts to extend the estimated instantaneous solar irradiance to the daily global SSI (Bisht et al., 2005; Kambezidis et al., 2017; Psiloglou et al., 2020). Since the plotted variation in daily SSI is similar to the shape of a downward parabola, some researchers employed quadratic polynomial regression to estimate the daily SSI from Terra/MODIS and Aqua/MODIS products (Xu et al., 2016; Yan et al., 2018). However, the SSI varies throughout the daytime with the solar zenith angle and atmospheric conditions, especially under cloudy weather conditions, and the polar-orbiting satellites mentioned above cannot effectively reflect these changes due to their limited observation intervals (once or twice a day). Compared with polar-orbiting satellites, geostationary satellites have unique advantages in obtaining the diurnal variation characteristics of SSI owing to their high temporal resolution (Zhang et al., 2011; Tang et al., 2016; Peng et al., 2020; Letu et al., 2020). However, traditional geostationary meteorological satellite products have relatively low spatial and spectral resolutions, making it difficult to accurately obtain the contents of the main atmospheric components, such as clouds, aerosols, and water vapor, which strongly attenuate solar irradiance and exhibit rapid diurnal changes at a regional scale.

Himawari-8, a new-generation geostationary meteorological satellite, was launched by the Japan Meteorological Agency on October 7, 2014. It acquires full-disk observations in 16 multispectral bands (3 visible, 3 near-infrared, and 10 infrared bands), offering great promise in monitoring aerosols and clouds for the accurate estimation of SSI (Bessho et al., 2016). The Himawari-8 SSI products have attracted considerable attention because of their high temporal resolution (2.5 minutes-10 minutes) and high spatial resolution (0.5 km-2 km), which enable renewed research on the spatiotemporal distribution of solar irradiance. Some scholars verified the 10-minute, hourly, daily average, and monthly average radiation products of Himawari-8 and reported that these SSI datasets agree well with ground measurements (Bessho et al., 2016; Damiani et al., 2018; Shi et al., 2018; Yu et al., 2018).

In this study, a pixel-by-pixel Gaussian fitting method is explored to estimate the daily global SSI from Himawari-8 hourly products. This approach uses the least-squares method to find the ideal dynamic parameters based only on satellite products and overcomes the need to acquire input empirical parameters and the reliance on ground observations.

* Corresponding author.
E-mail address: zyl0322@nwnu.edu.cn(Y. Zhang).

2. DATA

2.1 Himawari-8 SSI products

The area observed by Himawari-8 ranges from 60°S to 60°N and from 80°E to 160°W. Hourly and 10-minute SSI products with a spatial resolution of 5 km were chosen for this study. To investigate the variation in solar irradiance over China throughout the year, the Himawari-8 radiation products from March 1, 2016, to February 28, 2017, were selected, covering approximately 9000 scenes in combination with available ground observations. Furthermore, when Himawari-8 hourly radiation data are not available because of missing values, the average values of the 10-minute products corresponding to the hour with missing data are used to compensate. The Himawari-8 SSI products used in this study are provided by the Japan Aerospace Agency (JAXA) (https://www.eorc.jaxa.jp/ptree/).

2.2 Ground-based measurements

The verification data were derived from the China radiation daily value dataset from the China Meteorological Data Network (http://data.cma.cn/). The quality of all measured ground-based SSI data is controlled and reported by the China Meteorological Administration (CMA) (Shi et al., 2008; Tang et al., 2011). To improve the credibility of the accuracy verification, 64 radiation stations with complete annual field observations were selected from among 99 national radiation stations, where the remaining stations were not chosen because they had missing observations from March 2016 to February 2017. The spatial distribution of the selected 64 ground observation stations is shown in Figure 1.

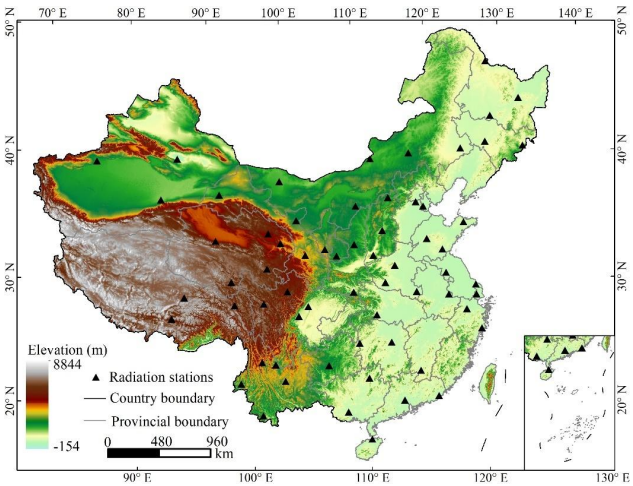

Figure 1. Spatial distribution of the 64 ground-based radiation stations over China.

In addition, we explored the reasons for the differences in the goodness of fit of the curves under different weather conditions. It is necessary to compare the hourly SSI measured on the ground with the Himawari-8 hourly radiation products and Gaussian fitting values. This study also uses radiation observations provided by the Heihe Watershed Allied Telemetry Experimental Research (HiWATER) dataset of the Hydrometeorological Observation Network (automatic weather station of the Heihe remote sensing station), acquired on August 24, 29, and 30, 2016; these data, provided by the Cold and Arid Regions Scientific Data Center (http://westdc.westgis.ac.cn/), have already been processed and quality controlled (Liu et al., 2011; 2018). To be consistent with the time scale of the Himawari-8 SSI products, the ground-based measurements collected at a 10-minute interval were aggregated into 1-hour averages.

Therefore, four kinds of SSI datasets are used in this study: two (hourly and 10-minute) Himawari-8 radiation products and in situ observations of two meteorological staions, as shown in Table 1. It should be noted that the time of all data mentioned in this article is BJT unless otherwise noted.

SSI data source	Spatial resolution	Temporal resolution	Date (days)
Himawari-8	5 km	hourly	2016/03-2017/02 (365)
		10-minute	2016/6/21 (1)
CMA	-	daily	2016/03-2017/02(365)
HiWATER		10-minute	2016/08/24, 29, 30 (3)

Table 1. Details of the data products used in this research.

3. METHODS

Some studies confirmed that diurnal SSI variations obey a Gaussian distribution (Yao et al., 2015; Ayvazoğluyüksel and Filik, 2018). In this study, a pixel-by-pixel Gaussian fitting method based on the least-square principle is proposed to estimate the daily global SSI from the Himawari-8 hourly SSI products. As shown in Figure 2, the estimation process includes three main steps: Radiation data extraction during the daytime, fitting the Gaussian curve pixel by pixel according to the hourly radiation products during the daytime, and integration according to the parameters derived from the Gaussian fitting curve.

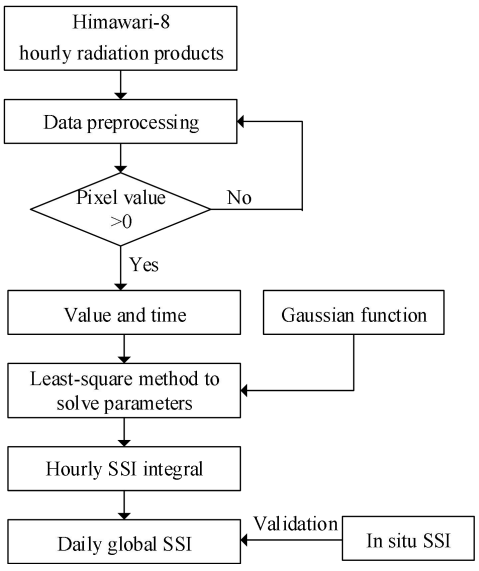

Figure 2. Flowchart of estimating the daily global SSI from the Himawari-8 hourly radiation products.

3.1 Radiation data extraction during the daytime

To perform Gaussian fitting in each pixel, two types of input parameters are required: the satellite transit time and corresponding pixel value of the Himawari-8 hourly daytime SSI. However, we must pay attention to the data extraction error of Himawari-8 hourly SSI during the daytime caused by the 8-hour difference between BJT (UTC+8) and UTC. For example,

the SSI products in China on June 22 should be chosen from 16:00 on June 21 to 16:00 on June 22 in UTC, instead of 0:00 to 24:00 on June 22. As shown by the red ellipses in Figure 3, otherwise, it will bring about large errors when the atmospheric conditions on adjacent two days are very different, especially between sunrise and 08:00. The time zone difference also illustrates the fact that the daily average solar irradiance of Himawari-8 products in UTC cannot be directly converted into the daily global SSI in China.

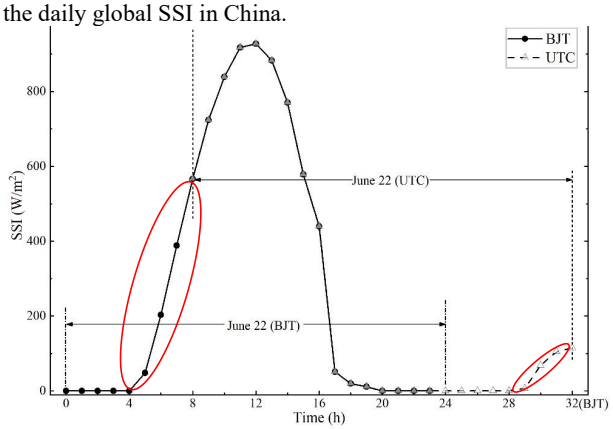

Figure 3. Hourly SSI variation in China (longitude: 117.03°E, latitude: 39.05°N) under UTC and BJT on June 22, 2016.

3.2 Fitting the Gaussian curve pixel by pixel

Previous studies demonstrated that a dozen discrete hourly observations of solar irradiance obtained by Himawari-8 during the daytime cannot be used to accurately estimate the daily global SSI. Therefore, it is necessary to find a Gaussian fitting curve to simulate the actual distribution characteristics of the solar irradiance. The Gaussian fitting curve is established by retrieving the dynamic parameters pixel by pixel according to the Himawari-8 hourly SSI. At a point on the Gaussian curve, the solar irradiance is marked as R_t (W/m^2, R_t> 0), which is calculated by the following Gaussian function:

$$R_t = ae^{\frac{-(t-b)^2}{c^2}} \quad (1)$$

where t signifies any moment between the time of the satellite product corresponding to the period from sunrise to sunset and R_t represents the fitted value of SSI at a given time t. a, b, and c are the three unknown dynamic parameters, which vary with time, space, and weather conditions.

To apply the Gaussian curve to fit the variation in solar irradiance of each pixel during the daytime, the parameters a, b, and c are estimated according to the principle of the least-squares method (Marquardt, 1963) to enable the R_t value at any point on the fitted curve to best match the discrete observation y_t obtained by Himawari-8. The difference between the estimated value and the observed value is defined as an error, and its sum of squares is expressed as S, which is required to satisfy the following equation:

$$S = \sum_{t=i}^{n} \left[R_t - y_t\right]^2 = \mathrm{MIN} \quad (2)$$

In order to achieve the minimum (MIN) value of S, an iterative solution is adopted, and the dynamic parameters a, b, and c are determined by using the Python programming language.

3.3 Estimation of the daily global SSI

By substituting the Himawari-8 hourly radiation products during the daytime into a Gaussian function, the undetermined parameters of the Gaussian curve for each pixel can be obtained by using the least-square principle, which can capture the diurnal variation characteristics of solar irradiance. Then, the Gaussian fitting curves are integrated to estimate the daily global SSI pixel by pixel using Eq. (3) based on the Himawari-8 hourly radiation products:

$$R_d = \left(\int_{\Delta T} R_t d_t \right) \times 3600 / 1000000 \quad (3)$$

where R_d represents the daily global SSI estimate (MJ/m^2); $_\Delta T$ is the integration period, which corresponds to the length of daytime; and 3600/1000000 is the solar irradiance unit conversion coefficient for converting the Himawari-8 hourly radiation products (W/m^2) into daily global solar irradiance (MJ/m^2). Another advantage of this radiation unit conversion is that the estimated daily global solar irradiance has the same units as the ground measurements, which is also convenient for verifying the accuracy.

4. RESULTS

4.1 Accuracy verification

The estimated daily global SSI was evaluated against ground measurements from 64 CMA stations. Three statistical metrics were selected to evaluate the accuracy, namely, the mean bias error (MBE), RMSE, and coefficient of determination (R^2), the formulas for which are detailed in Huang et al. (2012). As shown in Figure 4, the estimated daily global SSI and the observed daily global SSI in this study have relatively high consistency, with the R^2 value exceeding 0.86 on both all-sky and clear-sky days, which indicates that the proposed Gaussian fitting method can be used for estimating daily global SSI. Under all-sky conditions, a total of 23360 sample points at 64 ground radiation sites display a positive MBE of 0.87 MJ/m^2, an RMSE of approximately 3.06 MJ/m^2, and an R^2 of approximately 0.86. The estimated accuracy on clear-sky days is better than that on all-sky days with a smaller RMSE (2.36 MJ/m^2) and a higher R^2 (0.91).

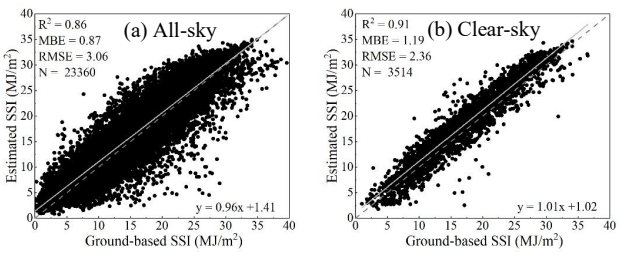

Figure 4. Scatter plots comparing the estimated SSI with the ground-measured daily global SSI. (a) Daily global values on all-sky days and (b) daily global values on clear-sky days.

Although the estimated daily global SSI has high accuracy, the error statistic exhibits considerable spatial heterogeneity, shown as in Figure 5. The spatial distribution of the statistic error shows that the SSI errors in Northwest China are the lowest, while the errors are relatively high in the southern regions and the Qinghai-Tibet Plateau. The largest negative deviation in the MBE is distributed mainly in the Qinghai-Tibet region, which

indicates that the Gaussian fitting method underestimates the daily global SSI in this area. Shi et al. (2018) showed that the atmospheric profile parameters in the radiation transmission model for the production of Himawari-8 products come from the 2013 Japan Global Spectral Model, which inaccurately estimates the water vapour, aerosols, and other components with low extinction rates, potentially leading to the underestimation of solar irradiance in the Qinghai-Tibet Plateau.

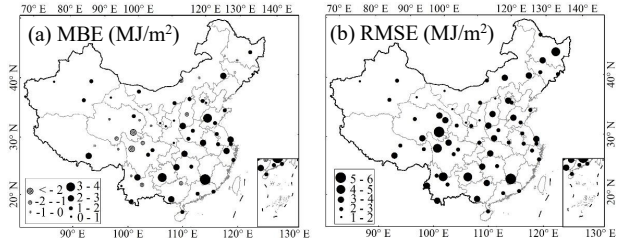

Figure 5. Distributions of the error statistics of the daily global SSI estimated from March 2016 to March 2017.

Moreover, the daily global solar irradiance estimated in East and Southeast China is higher than the ground measurements, which may be caused by heavy cloud cover and dense aerosols. Tang et al. (2016) pointed out that the satellite-retrieved SSI in southern China overestimates the ground-measured values because of the low accuracy of cloud parameters obtained under broad cloud cover and rapid changes in the region. Furthermore, the eastern regions of China suffer from high aerosol contents due to the rapid economic development and booming population growth therein, and such high contents may lead to uncertainty in the SSI estimation. Li et al. (2019) used ground-observed aerosols to evaluate the Himawari-8 aerosol products in eastern China and proposed that surface aerosols therein were underestimated, especially in East China. In contrast, the estimation errors in Central and Northwest China are smaller than those in other regions because of the limited precipitation and abundance of clear-sky days.

4.2 Mapping of daily global SSI

The global solar irradiances in China of 365 days from March 2016 to March 2017 were estimated by Gaussian fitting based on Himawari-8 hourly radiation products. To analyse the spatial distribution characteristics of the daily global SSI in China, the autumnal equinox (September 23) in 2016 was selected. As shown as in Figure 6, the values of daily global SSI show strong spatial heterogeneity. Affected by cloudy conditions and rainfall, the Qinghai-Tibet Plateau, Southwest China, and Northeast China have lower daily global SSI than other regions. Conversely, higher daily global SSI is observed in Northwest, North, and Southeast China. These experimental results are highly consistent with the local weather historical records on September 23, 2016.

Figure 7 investigates diurnal variability of the Himawari-8 hourly SSI from 06:00 to 20:00 in BJT on the autumnal equinox in 2016. It can be seen that the hourly solar irradiance values tend to form west-east contours in the morning and east-west contours in the afternoon. With increasing solar altitude angle, the solar irradiance value gradually increases, reaching a peak at approximately 12:00 local time. Generally, lower-latitude and higher-altitude regions can receive more solar irradiance; however, the spatial distribution of SSI also changes with the local atmospheric conditions (such as the movement of clouds) and topography. Combining Figure 6 with Figure 7 reveals that the variation in hourly SSI at approximately noon (local time) contributes greatly to the daily global SSI; that is, the spatial distribution of daily global SSI is similar to that of solar irradiance at approximately noon. These experimental results demonstrate that the Qinghai-Tibet Plateau is in a low solar irradiance area due to the influence of clouds. Previous studies noted that the Qinghai-Tibet Plateau is a stable high-value region of seasonal and annual SSI changes in China (Lu et al., 2010; Tang et al., 2016).

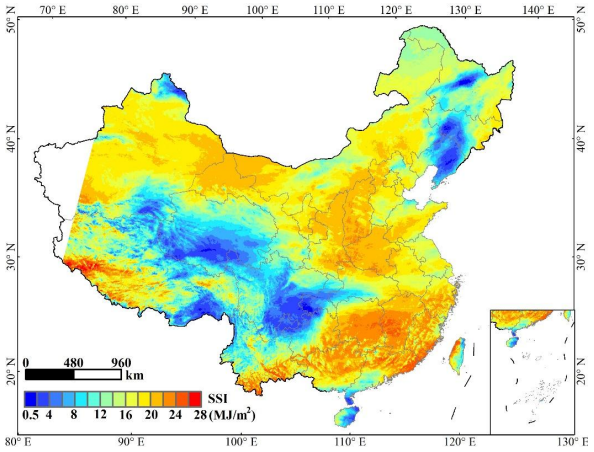

Figure 6. Spatial distribution of the daily global SSI estimated by the Gaussian fitting method on September 23, 2016.

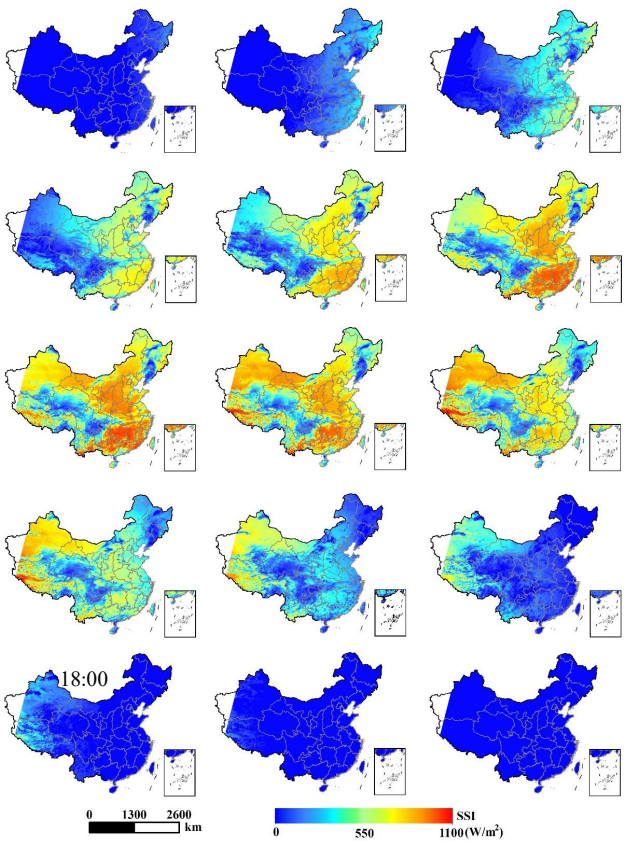

Figure 7. Diurnal variability of the Himawari-8 hourly SSI from 06:00 to 20:00 in BJT on September 23, 2016.

China's territory is vast, and thus, the spatial distribution of daily global SSI displays obvious regional and seasonal differences due to differences in the local topography and climatic environment of each region. Therefore, it is necessary to expand the daily global solar irradiance on the seasonal and

annual scales to obtain the spatial and temporal distributions of the seasonal average daily global solar irradiance and the annual average daily global solar irradiance, respectively. Experiments have shown obvious spatial heterogeneity in both annual and seasonal daily global solar irradiance. In general, the daily global solar irradiance at high elevations is higher than that at low elevations, and that in dry areas is higher than that in humid areas. Figure 8 (a) shows the annual average daily global SSI distribution over China, indicating that the daily global SSI in the Sichuan Basin is always low due to the low elevation and high cloud cover throughout the year.

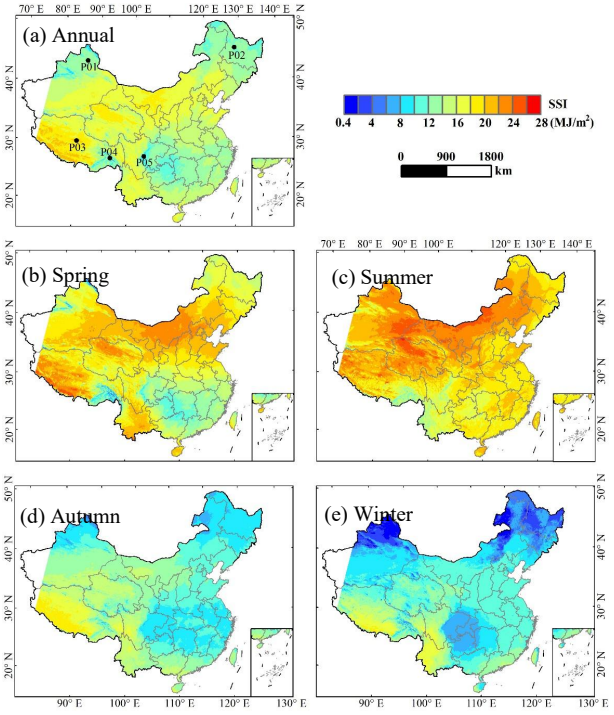

Figure 8. Spatial distributions of the annual and seasonal average daily global SSI variations in China from March 2016 to February 2017.

As shown in Figure 8 (b)-(e), the daily global SSI has obvious seasonal variation characteristics due to the influences of the solar elevation and sunshine duration. This finding demonstrates that the daily global solar irradiance gradually increases from spring to summer but gradually decreases from summer to winter. Overall, the daily global SSI in summer is the highest, with an average of 20.40 MJ/m^2, while that in winter is the lowest, with an average of 9.70 MJ/m^2. In addition, in autumn and winter, the daily global SSI in Northeast and Northwest China is extraordinarily lower than that in other regions due to the influence of latitude.

To further analyze the spatiotemporal differences of daily global SSI variation in China, five representative points, namely P01, P02, P03, P04, and P05 in Figure 8 (a), were selected according to the analysis of annual and season radiation variation. Figure 9 shows the spatiotemporal variation of the monthly average daily global SSI at 5 points. The monthly average daily global SSI variation trend of these points is similar on the whole, but there are some differences among the 5 points. The radiation value at point P03 in the Qinghai-Tibet Plateau is the highest throughout the year due to its high altitude and low cloud cover, while that point at P04 in the southeast of the Qinghai-Tibet Plateau is very low during the same period because of its affected by the southwest monsoon and topography. The monthly average daily global SSI at points P01 and P02 in the Northwest and Northeast China were high from March to November, but due to the influence of latitude, the radiation energy received from November to February of the following year were lower than those received at the other three points.

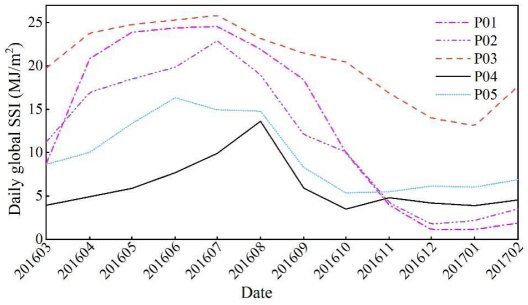

Figure 9. Monthly variation of daily global SSI in different regions of China from March 2016 to February 2017.

5. DISCUSSION

5.1 Comparison of the daily global SSI estimated by 10-minute products

Considering the computational efficiency, in this study, the daily global SSI is estimated from the Himawari-8 hourly radiation products rather than from the 10-minute products. In theory, the 10-minute radiation products can better reflect the characteristics of the daily global SSI received by the Earth's surface on a given day than can the hourly radiation products. To compare the daily global solar irradiance difference estimated by these two Himawari-8 radiation products, the hourly and 10-minute radiation products on a certain day are randomly selected. Figure 10 (a) and Figure 10 (b) illustrate the spatial distributions of the daily global SSI estimated from the hourly and 10-minute radiation products, respectively, on August 21, 2016. The results of this comparison indicate that the daily global SSI estimated from the Himawari-8 hourly radiation products is similar to that estimated from the 10-minute radiation products. In most regions, the deviation between the daily global SSI estimated from these two radiation products is within 0.5 MJ/m^2, and the average deviation is 0.12 MJ/m^2 (Figure 10 (c)). Overall, the daily global SSI value estimated with the Himawari-8 hourly radiation products is slightly higher than that estimated from the 10-minute products. Since the validation results in Section 4.1 show that the hourly products overestimate the daily global SSI, using the 10-minute radiation products may slightly improve the daily global SSI estimation accuracy.

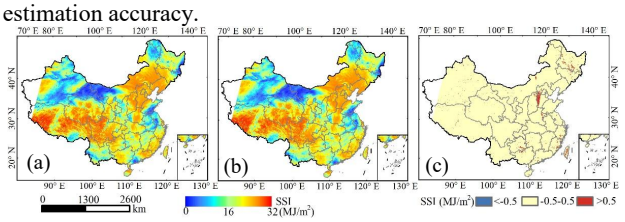

Figure 10. Spatial distributions of the estimated daily global SSI from the Himawari-8 hourly and 10-minute radiation products on August 21, 2016, as well as a map of the corresponding differences: (a) estimation from hourly products, (b) estimation from 10-minute products, and (c) the difference in the daily global SSI estimated from the hourly and 10-minute radiation products.

This contribution has been peer-reviewed. The double-blind peer-review was conducted on the basis of the full paper.
https://doi.org/10.5194/isprs-annals-V-3-2022-493-2022 | © Author(s) 2022. CC BY 4.0 License.

5.2 Comparison between the Gaussian fitting and quadratic polynomial regression methods

The quadratic polynomial regression method is also widely used to extrapolate the temporal distribution of daily global SSI. Comparing the results of the Gaussian fitting method with those of quadratic polynomial regression can further verify the rationality of the former. Therefore, 4 representative days out of the year from the Himawari-8 hourly radiation products and the corresponding ground measurements at 64 sites are selected. The four selected days are March 20, June 21, September 22, and December 21 in 2016, representing spring, summer, autumn, and winter, respectively.

Date	Gaussian fitting			Quadratic polynomial		
	MBE	RMSE	R^2	MBE	RMSE	R^2
2016/03/20	1.95	3.48	0.80	2.27	3.65	0.80
2016/06/21	0.51	3.80	0.77	0.90	3.82	0.78
2016/09/22	1.08	2.94	0.75	1.42	3.04	0.76
2016/12/21	1.14	1.60	0.93	1.28	1.73	0.93
Total	1.17	3.06	0.87	1.47	3.16	0.87

Table 2. Comparison between the Gaussian fitting and uadratic polynomial methods (MJ/m2)

The statistics in Table 2 demonstrate that the daily global solar irradiance estimates by the two methods are highly correlated with the ground observations in different seasons, with an R^2 of approximately 0.87. However, both methods overestimate the solar irradiance received on the ground, but the overestimate of the quadratic polynomial method (MBE=1.47 MJ/m^2) is larger than that of the Gaussian fitting method (MBE=1.17 MJ/m^2). Moreover, the RMSE of the Gaussian fitting method is 3.06 MJ/m^2, which is smaller than 3.16 MJ/m^2 of the quadratic polynomial method, and the MBE and RMSE estimated by the Gaussian fitting method are both smaller than those estimated by the quadratic polynomial method. These results all indicate that the Gaussian fitting method has high stability and can estimate daily global solar irradiance more accurately than quadratic polynomial regression.

5.3 Uncertainty analysis of the daily global SSI estimation

Our experiments confirm that the pixel-by-pixel Gaussian fitting method based on the least-squares method can accurately estimate daily global solar irradiance, but this method also has certain limitations. With the aim of analysing the estimation uncertainty, the SSI estimated under different weather conditions is compared with concurrent ground observations. Figure 11 demonstrates that the estimation curve is basically consistent with the variation curves of the field measurements and the Himawari-8 hourly radiation products on a clear-sky day (Figure 11 (c)). However, under cloudy and rainy conditions, the difference between the curves of the Himawari-8 hourly SSI and the ground observations increases, which increases the difference between the Gaussian fitting curve and the variation curve of the ground observations. Obviously, there is large uncertainty in the Gaussian fitting method under complex atmospheric conditions, which reduces the solar irradiance estimation accuracy.

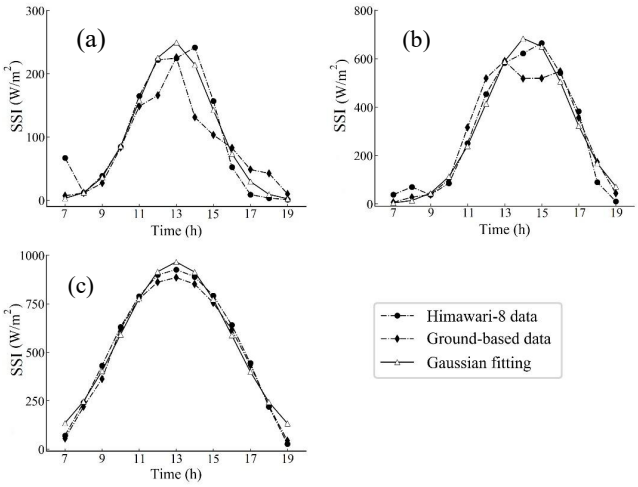

Figure 11. Variation curves of the proposed Gaussian fitting method, the ground-based measurements from Heihe remote sensing stations, and the Himawari-8 hourly SSI products under different weather conditions in 2016: (a) moderately rainy day on August 24; (b) cloudy conditions on August 29; and (c) clear-sky conditions on August 31.

The estimation accuracy also involves an authenticity verification of the ground measurements corresponding to the remote sensing product pixels. In this verification method, there are differences in the matching at the temporal and spatial scales between the Himawari-8 hourly SSI products and ground measurements. At the spatial scale, the estimated daily global solar irradiance represents the average radiation energy in the planar range of several square kilometres, while the ground measurements represent only the radiation in a very small range centred on the observation point. At the temporal scale, the Himawari-8 hourly radiation products are generated from transient instantaneous satellite observations, while ground measurements are cumulative over time. At certain temporal and spatial scales, the instantaneous values observed by satellites can represent the values in a specified period or on a certain plane under stable weather conditions. However, these observations cannot represent a certain time or a specified location due to the variability of clouds and relative humidity under cloudy and rainy conditions. Therefore, the spatiotemporal differences between satellite observations and ground measurements will degrade the performance of the Gaussian fitting method when estimating the daily global SSI from Himawari-8 hourly radiation products under complex weather conditions.

6. CONCLUDION

Due to the 8-hour time lag between BJT and UTC, a large error is encountered when calculating the daily global solar irradiance in China by using the Himawari-8 daily average radiation products released in UTC. Moreover, the Himawari-8 10-minute radiation product has a large data volume because of its high temporal resolution. Thus, to balance the estimated efficiency and accuracy of the daily global SSI, Himawari-8 hourly radiation products are selected to calculate the daily global SSI in China.

A pixel-by-pixel Gaussian fitting method based on the least-square principle was proposed to estimate the daily global SSI from Himawari-8 hourly radiation products and was proven

effective in this study. A total of 23360 sample points from 64 stations were selected to evaluate the accuracy. The validation results reveal R^2 values greater than 0.86 under all-sky and clear-sky conditions, and the estimation results under clear-sky conditions (MBE is 1.19 MJ/m^2 and RMSE is 2.36 MJ/m^2) are better than those under all-sky conditions (MBE is 0.87 MJ/m^2 and RMSE is 3.06 MJ/m^2). Compared with the widely used quadratic polynomial and accumulation methods, the daily global SSI estimated by Gaussian fitting has higher accuracy and good stability. In general, the daily global SSI spatial distribution exhibits high heterogeneity due to the influences of local terrain and atmospheric conditions. High-elevation areas with low cloud cover, such as the Qinghai-Tibet Plateau, Inner Mongolia, and Northwest China, have a higher daily global SSI than other regions. In contrast, the daily global SSI is relatively low in the eastern regions of Southwest and Northeast China due to their low elevations and severe cloud cover or short sunshine durations. Moreover, the estimation accuracy of the daily global SSI from Himawari-8 hourly radiation products is similar to that based on 10-minute radiation products.

This study proposed an effective method for calculating daily global SSI from satellite hourly SSI products, which is of great significance for future research on climate, ecology, and solar energy resources. However, this research has some shortcomings, such as the low estimation accuracy under cloudy-sky days, only one year for the experimental dataset, sparse ground observation sites, and a simple verification method. In future research, the influence of cloud cover, topography and other factors should be considered to further improve the accuracy of daily global SSI estimation.

ACKNOWLEDGEMENTS

This research was supported by the National Natural Science Foundation of China (NSFC) project, grant number 41871277 and number 41561080, and the China Postdoctoral Fund project grant number 2016M602893. The authors would like to thank the China Meteorological Administration (CMA) and the Cold and Arid Regions Scientific Data Center for providing the ground-measured global radiation data and the Japan Aerospace Exploration Agency (JAXA) for the public radiation products produced from Himawari-8.

REFERENCES

Ayvazoğluyüksel, Ö., Filik, Ü. B., 2018. Estimation methods of global solar radiation, cell temperature and solar power forecasting: A review and case study in Eskişehir. *Renewable and Sustainable Energy Reviews*, 91, 639-653. https://doi.org/10.1016/j.rser.2018.03.084.

Bisht, G., Venturini, V., Islam, S., Jiang, L., 2005. Estimation of the net radiation using MODIS (moderate resolution imaging spectroradiometer) data for clear sky days. *Remote Sensing of Environment*, 97(1), 52-67. https://doi.org/10.1016/j.rse.2005.03.014.

Bessho, K., Date, K., Hayashi, M., Ikeda, A., Imai, T., Inoue, H., Okuyama, A., 2016. An introduction to Himawari-8/9—Japan's new-generation geostationary meteorological satellites. *Journal of the Meteorological Society of Japan. Ser. II*, 94(2), https://doi.org/151-183. 10.2151/jmsj.2016-009.

Damiani, A., Irie, H., Horio, T., Takamura, T., Khatri, P., Takenaka, H., Cordero, R. R., 2018. Evaluation of Himawari-8 surface downwelling solar radiation by ground-based measurements. *Atmospheric Measurement Techniques*, 11(4), 2501-2521. https://doi.org/10.5194/amt-2017-440.

Huang G., Liu S., Liang S., 2012. Estimation of net surface shortwave radiation from MODIS data. *International Journal of Remote Sensing*, 33(3), 804-825. https://doi.org/10.1080/01431161.2011.577834.

Huang, G., Li, Z., Li, X., Liang, S., Yang, K., Wang, D., Zhang, Y., 2019. Estimating surface solar irradiance from satellites: Past, present, and future perspectives. *Remote Sensing of Environment*, 233, 111371. https://doi.org/10.1016/j.rse.2019.111371.

Journée, M., Bertrand, C., 2010. Improving the spatio-temporal distribution of surface solar radiation data by merging ground and satellite measurements. *Remote Sensing of Environment*, 114(11), 2692-2704. https://doi.org/10.1016/j.rse.2010.06.010.

Kambezidis, H., Psiloglou, B., Karagiannis, D., Dumka, U., Kaskaoutis, D., 2017. Meteorological Radiation Model (MRM v6. 1): Improvements in diffuse radiation estimates and a new approach for implementation of cloud products. *Renewable and Sustainable Energy Reviews*, 74, 616-637. https://doi.org/10.1016/j.rser.2017.02.058.

Letu, H., Yang, K., Nakajima, T. Y., Ishimoto, H., Nagao, T. M., Riedi, J., Khatri, P., 2020. High-resolution retrieval of cloud microphysical properties and surface solar radiation using Himawari-8/AHI next-generation geostationary satellite. *Remote Sensing of Environment*, 239, 111583. https://doi.org/10.1016/j.rse.2019.111583.

Li, D., Qin, K., Wu, L., Xu, J., Letu, H., Zou, B., Li, Y., 2019. Evaluation of JAXA Himawari-8-AHI Level-3 Aerosol Products over Eastern China. *Atmosphere*, 10(4), 215. https://doi.org/10.3390/atmos10040215.

Liu, S., Xu, Z., Wang, W., Jia, Z., Zhu, M., Bai, J., Wang, J., 2011. A comparison of eddy-covariance and large aperture scintillometer measurements with respect to the energy balance closure problem. *Hydrology and Earth System Sciences*, 15(4), 1291-1306. https://doi.org/10.5194/hess-15-1291-2011.

Liu, S.M., Li, X., Xu, Z., Che, T., Xiao, Q., Ma, M., Ren, Z., 2018. The Heihe Integrated Observatory Network: A Basin-Scale Land *Surface Processes Observatory in China.* Vadose Zone Journal, 17(1). https://doi.org/10.2136/vzj2018.04.0072.

Lu, N., Liu, R., Liu, J., Liang, S., 2010. An algorithm for estimating downward shortwave radiation from GMS 5 visible imagery and its evaluation over China. *Journal of Geophysical Research: Atmospheres*, 115(D18). https://doi.org/10.1029/2009JD013457.

Marquardt, D. W., 1963. An Algorithm for least-squares estimation of nonlinear parameters. *Journal of The Society for Industrial and Applied Mathematics*, 11(2), 431-441. https://doi.org/10.1137/0111030.

Peng, Z., Letu, H., Wang, T., Shi, C., Zhao, C., Tana, G., Shi, J., 2020. Estimation of shortwave solar radiation using the artificial neural network from Himawari-8 satellite imagery over China. *Journal of Quantitative Spectroscopy and Radiative Transfer*, 240, 106672. https://doi.org/10.1016/j.jqsrt.2019.106672.

Psiloglou, B., Kambezidis, H., Kaskaoutis, D., Karagiannis, D., Polo, J. M., 2020. Comparison between MRM simulations, CAMS and PVGIS databases with measured solar radiation components at the Methoni station, Greece. *Renewable energy*, 146, 1372-1391. https://doi.org/10.1016/j.renene.2019.07.064.

Shi, G. Y., Hayasaka, T., Ohmura, A., Chen, Z. H., Wang, B., Zhao, J. Q., Xu, L., 2008. Data quality assessment and the long-term trend of ground solar radiation in China. *Journal of Applied Meteorology and Climatology*, 47(4), 1006-1016. https://doi.org/10.1175/2007JAMC1493.1.

Shi, H., Li, W., Fan, X., Zhang, J., Hu, B., Husi, L., Xia, X., 2018. First assessment of surface solar irradiance derived from Himawari-8 across China. *Solar Energy*, 174, 164-170. https://doi.org/10.1016/j.solener.2018.09.015.

Tang, W., Yang, K., Qin, J., Cheng, C., He, J., 2011. Solar radiation trend across China in recent decades: a revisit with quality-controlled data. *Atmospheric Chemistry and Physics*, 11(1), 393-406. https://doi.org/10.5194/acpd-10-18389-2010.

Tang, W.J., Qin, J., Yang, K., Liu, S., Lu, N., Niu, X., 2016. Retrieving high-resolution surface solar radiation with cloud parameters derived by combining MODIS and MTSAT data. *Atmospheric Chemistry and Physics*, 16(4), 2543-2557. https://doi.org/10.5194/acp-16-2543-2016.

Xu, X., Du, H., Zhou, G., Mao, F., Li, P., Fan, W., et al., 2016. A method for daily global solar radiation estimation from two instantaneous values using MODIS atmospheric products. *Energy*, 111, 117-125. https://doi.org/10.1016/j.energy.2016.05.095.

Yan, G., Tong, Y., Yan, K., Mu, X., Chu, Q., Zhou, Y., Zhou, H., 2018. Temporal extrapolation of daily downward shortwave radiation over cloud-free rugged terrains. Part 1: Analysis of topographic effects. *IEEE Transactions on Geoscience and Remote Sensing*, 56(11), 6375-6394. https://doi.org/10.1109/TGRS.2018.2838143.

Yang, K., Koike, T., 2005. A general model to estimate hourly and daily solar radiation for hydrological studies. *Water Resources Research*, 41(10). https://doi.org/10.1029/2005WR003976.

Yao, W., Li, Z., Xiu, T., Lu, Y., Li, X., 2015. New decomposition models to estimate hourly global solar radiation from the daily value. *Solar Energy*, 120, 87-99. https://doi.org/10.1016/j.solener.2015.05.038.

Yu, Y., Shi, J., Wang, T., Letu, H., Yuan, P., Zhou, W., Hu, L., 2018. Evaluation of the Himawari-8 Shortwave Downward Radiation (SWDR) Product and its Comparison With the CERES-SYN, MERRA-2, and ERA-Interim Datasets. *IEEE Journal of Selected Topics in Applied Earth Observations and Remote Sensing*, 12(2), 519-532. https://doi.org/10.1109/JSTARS.2018.2851965.

Zhang, H., Xin, X., Liu, Q., 2011. Modeling daily net shortwave radiation over rugged surfaces using MODIS atmospheric products. *IEEE International Geoscience and Remote Sensing Symposium. Ieee*, 3787-3790. https://doi.org/10.1109/IGARSS.2011.6050055.

Zhang, Y., Qin, X., Li, X., Zhao, J., Liu, Y., 2020. Estimation of Shortwave Solar Radiation on Clear-Sky Days for a Valley Glacier with Sentinel-2 Time Series. *Remote Sensing*, 12(6), 927. https://doi.org/10.3390/rs12060927.

Zou, L., Wang, L., Li, J., Lu, Y., Gong, W., Niu, Y., 2019. Global surface solar radiation and photovoltaic power from Coupled Model Intercomparison Project Phase 5 climate models. *Journal of Cleaner Production*, 224, 304-324. https://doi.org/10.1016/j.jclepro.2019.03.268.